LRP 425/90 December 1990

TUNABLE INTEGRATION SCHEME FOR THE FINITE ELEMENT METHOD

A. Bondeson and G.Y. Fu

TUNABLE INTEGRATION SCHEME FOR THE FINITE ELEMENT METHOD

A. Bondeson and G.Y. Fu

Centre de Recherches en Physique des Plasmas, Association Euratom - Confédération Suisse,
Ecole Polytechnique Fédérale de Lausanne, 21 Av. des Bains,
CH-1007 Lausanne, Switzerland

Abstract: A discretization method is proposed where a tunable integration scheme is applied to the finite element method (FEM). The method is characterized by one continuous parameter, p. Three different eigenvalue problems are used as test cases: a simple example with constant coefficients and two model problems from ideal and resistive magnetohydrodynamics. The numerical examples and a theoretical error analysis show that, for judicious choices of p, the tunable integration method clearly improves the accuracy of the strict FEM. The sensitivity to the choice of integration parameter is discussed.

1. INTRODUCTION

The finite element method (FEM) is commonly used to derive discrete equations for the numerical treatment of differential equations. The solution is approximated by expansion in a set of trial functions and the discrete equations for the expansion coefficients is obtained by taking the scalar product of the differential equation with appropriately chosen weighting functions. The integration involved in the scalar product is often carried out numerically. In this paper, we discuss how the integration method affects the accuracy of the solution and, in particular, how the accuracy of the solution can be *improved* by reducing the accuracy of the integration. The basic idea will be discussed for a simple second order differential equation with constant coefficients. Two model problems from magnetohydrodynamics (MHD) are considered in detail, but we believe that the technique may be useful also in other applications in physics and engineering.

Strang and Fix [1] addressed the question of how accurate the numerical integration needs to be to preserve the convergence rate of the FEM with exact integration. They showed that the integration scheme must be able to integrate exactly the highest derivative term appearing in the variational form. It is frequent practice to apply numerical integration schemes that are more accurate than this, but in the present paper we consider integration schemes where the error is of the same order as that of the FEM with exact integration. This means that the intrinsic FEM error can be balanced against the integration error to improve on convergence.

It is well known that for variational systems, strict FEM schemes lead to systematic errors in the estimate of eigenvalues. The approximation by a finite set of basis functions makes the system too 'stiff' in the mechanical sense. For unsuitable choices of test functions, the stiffness can be strongly deleterious and lead to serious degradation of accuracy known as 'locking' (see, e.g., Ref [2] and references therein) and 'spectral pollution' [3,4]. This can be avoided by the use of mixed elements [2-4] or staggered meshes [4,5]. An alternative remedy is offered by 'reduced' or 'selective' integration schemes of lower order [2]. In the present

paper, we are not concerned with cases of this type where very poor performance can be drastically improved by a change of test functions. Instead, we will show that even for appropriately chosen trial and weighting functions, the overall accuracy can be improved by deliberate introduction of inaccuracy in the integration. The error of the integration scheme can be chosen so as to balance the normal overestimation of the stiffness in the variational problem.

We apply the technique to three different eigenvalue problems solved by piecewise linear elements. The eigenvalues converge quadratically with mesh size when the integration is made using either the trapezoidal rule or the midpoint rule. The tunable integration method consists of choosing a linear combination of these two integration schemes, specified by a single continuous parameter, p. For particular values of this parameter, the resulting algorithm reproduces the standard FEM, the 'hybrid' finite elements of the ideal-MHD stability code ERATO [6] and finite differences. (Strictly speaking, the latter holds only for equations with constant coefficients.) The best convergence is generally *not* obtained from the standard FEM which uses the most accurate integration scheme, Simpson's rule.

Our test cases show that there is not a unique, optimal integration scheme valid for all systems. However, for each of the systems that we consider, clear improvement over the strict FEM result can be obtained by a judicious choice of p, and this optimal value is only weakly dependent on the system parameters.

In Sec. 2, we first illustrate the method for a simple, analytically solvable example. In Sec. 3, we give error estimates for a Sturm-Liouville eigenvalue problem. In Sec. 4 we apply the method to a selfadjoint model eigenvalue problem from ideal MHD and in Sec. 5 to its non-selfadjoint counterpart in resistive MHD.

2. INTEGRATION METHOD

The basic idea is best presented for a very simple example

$$\frac{d^2u}{dx^2} + \lambda u = 0 \quad . \qquad (1)$$

As this equation has constant coefficients, it has solutions of the form u = exp(ikx) and it is legitimate to consider λ as an eigenvalue for each k. We are interested in how the discretized approximation of the exact dispersion relation $\lambda = \lambda(k) = k^2$ depends on the grid spacing $h = x_{i+1} - x_i$ and the integration parameter p.

Equation (1) will be solved by the FEM, using piecewise linear elements on an equidistant mesh $x_i = i\,h$, i = .., -1, 0, 1,... . The approximate solution U is expanded in piecewise linear basis functions,

$$U(x) = \sum_{i=-\infty}^{\infty} U_i\, e_i(x) \quad . \qquad (2)$$

where $e_i(x)$ is the basis function that is 1 for $x = x_i$ and 0 on all other grid points. The discrete equations are obtained by multiplying (1) by arbitrary weighting functions V from the same space as U and integrating after partial integration of the first term.

We propose a scheme of tunable integration, where the integrals are carried out using a linear combination of the trapezoidal rule, multiplied by a parameter p and the midpoint rule, multiplied by 1-p, thus,

$$\int_{x_i}^{x_{i+1}} \phi(x)\,dx \approx (x_{i+1} - x_i) \left\{ \frac{p}{2} \left[\phi(x_i) + \phi((x_{i+1})] + (1-p)\, \phi\left(\frac{x_{i+1} + x_i}{2}\right) \right\} . \qquad (3)$$

The discretized equation obtained with the weighting function $V = e_i(x)$ is

$$(U_{i+1} - 2U_i + U_{i-1})/h^2 + \Lambda \left[U_i + \frac{1-p}{4} (U_{i+1} - 2U_i + U_{i-1}) \right] = 0 \quad , \qquad (4)$$

where Λ denotes the numerical estimate of the eigenvalue λ. It may be noted that p = 1 (trapezoidal rule) gives finite differences, p = 1/3 (Simpson's rule) gives the rigorous FEM

scheme, and p = 0 (midpoint rule) gives the hybrid finite elements [6]. The dispersion relation of the discretized equation (4) is

$$\Lambda = \frac{(4/h^2)\sin^2 kh/2}{1 - (1-p)\sin^2 kh/2} = k^2\left[1 + \left(\frac{2}{3} - p\right)\frac{k^2h^2}{4} + O(k^4h^4)\right] \qquad (5)$$

Equation (5) shows that FEM overestimates the eigenvalue and finite differences underestimate it, by equal amounts to $O(h^2)$. The hybrid element overestimate the eigenvalue more than FEM and have the disadvantage that $\Lambda \to \infty$ as $kh \to \pi$.

In this simple case, an optimal value for p is 2/3, which makes the $O(h^2)$ errors cancel, independent of k. This particular example has been discussed previously , e.g., in [2].

3. ERROR ESTIMATE FOR STURM-LIOUVILLE PROBLEM

We now derive an explicit error estimate for the eigenvalue of a Sturm-Liouville problem, including the integration error. For application to the test case in Sec. 4, we consider a slight generalization of the standard Sturm-Liouville problem

$$\frac{d}{dx} f(x,\lambda) \frac{du}{dx} - g(x,\lambda)\, u = 0 \quad , \quad a \le x \le b \quad ,$$
$$u'(a) - \alpha u(a) = 0 \quad , \quad u'(b) - \beta u(b) = 0 \quad , \qquad (6)$$

where both f and g can be functions of the eigenvalue λ. In Eq. (6), ' denotes d/dx and we assume that the condition $f(x, \lambda) > 0$ is satisfied.

The weak form of Eq. (6) is obtained by multiplying the differential equation by an arbitrary weighting function v and integrating in x. This defines a symmetric quadratic form which must vanish for any v in L_2

$$A(u, v; \lambda) = \int_a^b (fu'v' + guv)\, dx - \beta\, f(b, \lambda)\, u(b)v(b) + \alpha\, f(a, \lambda)\, u(a)v(a) = 0 \,. \quad (7)$$

We now consider the finite element solution of (6) on a grid x_i, i = 0, 1,..., n (not necessarily equidistant), with $x_0 = a$, $x_n = b$. The trial solution U and weighting function V are both expanded in piecewise linears

$$U(x) = \sum_{i=0}^{n} U_i\, e_i(x) \qquad V(x) = \sum_{i=0}^{n} V_i\, e_i(x) \quad .$$

For the discrete approximation of (6), we assume that the integral in (7) is carried out according to the tunable integration formula (3). We denote this numerical integration as

$$A_{appr}(U,V; \Lambda) = 0 \quad , \qquad (8)$$

where Λ is eigenvalue of the discretized system. Choosing V as the tent function that is 1 on a particular grid point i, and 0 on the others, we obtain the discrete equations for U_i, i = 0, 1, ..., n.

To proceed with the error analysis, we introduce an auxiliary function, $\boldsymbol{u}$. This function is chosen from the space of piecewise linears and is set equal to the exact solution u on the grid points

$$\boldsymbol{u}(x) = \sum_{i=0}^{n} u_i\, e_i(x)\,, \qquad u_i \equiv u(x_i) \quad . \qquad (9)$$

We can assert that $A_{exact}(u, U; \lambda) = 0$ because u solves the exact eigenvalue problem (6). Furthermore, $A_{appr}(\boldsymbol{u}, U; \Lambda) = 0$ because U solves (8) for any piecewise linear $V = \boldsymbol{u}$. Thus,

$$A_{appr}(\boldsymbol{u}, U; \Lambda) - A_{exact}(u, U; \lambda) = 0 \quad . \qquad (10)$$

The difference in the quadratic forms in (10) has three separate contributions, (1) the error in λ, $\delta\lambda = \Lambda - \lambda$, (2) the error due to numerical integration $\delta A = A_{appr} - A_{exact}$ and (3) the difference in the first argument $\delta u = \boldsymbol{u} - u$. These errors are all of order h^2, and to this order they can be estimated separately by writing (10) as

$$\delta\lambda \frac{\partial A_{exact}}{\partial\lambda}(u, u; \lambda) + \delta A(\boldsymbol{u}, U; \lambda) + A_{exact}(\delta u, U; \lambda) = O(h^4) . \qquad (11)$$

The third term in (11) represents an intrinsic FEM error which can be evaluated by noting that to $O(h^2)$, $A_{exact}(\delta u, U; \lambda) = A_{exact}(\delta u, \boldsymbol{u}; \lambda) = A_{exact}(\delta u, \delta u; \lambda)$. The other terms are simple to evaluate, and we arrive at the following formula for the $O(h^2)$ error in the eigenvalue

$$\delta\lambda = - E / I \quad ,$$

$$E = \frac{1}{12}\int_a^b f\, u''^2 h^2\, dx + \frac{1}{8}(p - \tfrac{1}{3})\int_a^b [(f''+2g)\, u'^2 + g''u^2 + 4g'uu']\, h^2\, dx , \qquad (12)$$

$$I = \int_a^b \left(\frac{\partial f}{\partial\lambda} u'^2 + \frac{\partial g}{\partial\lambda} u^2 \right) dx - \beta \frac{\partial f}{\partial\lambda} u^2(b) + \alpha \frac{\partial f}{\partial\lambda} u^2(a) \quad .$$

Equation (12) shows that the rigorous FEM (with $p = 1/3$ and $f > 0$) makes E positive. Thus, for the standard case $\partial f/\partial\lambda = 0$, $\partial g/\partial\lambda = -1$, (12) reproduces the well known result that FEM systematically overestimates the eigenvalue. The second term in E represents the integration error: it is proportional to $p - 1/3$.

For the introductory example of Sec. 2, the integration error comes from the λu term in (1), which gives a contribution proportional to $\int 2gu'^2\, dx = -2\lambda \int u'^2\, dx$ in E. It is easy to see that for $p = 2/3$, this integration error cancels the intrinsic FEM error term to lowest order.

The important conclusion that can be drawn from Eq. (12) is that integration errors can be introduced deliberately so as to balance the systematic error of the FEM. Two nontrivial, numerical examples will be given in the next two sections. Each of these two cases has a given

form, but the eigenvalue problem depends on certain parameters. Although the optimal p is different for the two systems, it is reasonably insensitive to the parameter values.

4. NUMERICAL EXAMPLE I - IDEAL MHD

We now apply the tunable integration scheme to the following equation with variable coefficients

$$\frac{d}{dx}(x^2 - \lambda)\frac{du}{dx} + Du = 0\,, \quad -1 \le x \le 1\,,$$
$$u'(-1) - \alpha u(-1) = 0\,, \quad u(1) = 0 \qquad . \tag{13}$$

Equation (13) arises in one-dimensional ideal-MHD stability problems from an expansion around the 'resonant surface' at x=0 [7]. The symbols in Eq. (13) have the following meaning: u denotes the fluid displacement perpendicular to the equilibrium magnetic surfaces, D is a constant proportional to the destabilizing pressure gradient in the direction of the field line curvature, and the eigenvalue λ is the square of the eigenfrequency. The condition $f = x^2 - \lambda > 0$ requires a negative λ, i.e., instability. For unstable eigensolutions, u shows non-trivial variations in an 'inertial layer' of width $(-\lambda)^{1/2}$. (For $0 < \lambda < 1$, there is a continuum of singular and un-normalizable eigenfunctions.)

It is useful to recall some basic properties of (13). First, when $D > 1/4$, the system (13) is locally unstable, i.e., it has an infinite number of negative eigenvalues independent of the boundary condition α. For global stability calculations, we are interested in the case $D < 1/4$, as the case $D > 1/4$ can be deemed unstable already by local stability criteria [8, 9]. Second, for $D < 1/4$, we find from the marginal stability analysis of Newcomb [7] that the system is unstable if $\alpha < 1/2 - (1/4 - D)^{1/2}$. The corresponding eigenmodes are *global*, since they depend on the boundary condition.

Figure 1 shows convergence curves for the numerical eigenvalue Λ vs. $h^2 = 4/N^2$ (where N is the number of cells) for three different cases. These results were obtained by applying the tunable integration scheme (3) to (13) on a uniform grid. The eigenvalues converge quadratically and the $O(h^2)$ error varies linearly with p, as predicted by (12). The parameter values are: in case (a), D = - 0.1 and α = - 0.13 and in case (b), D = 0.1 and α = 0.06. For these two cases, the value of p that minimizes the $O(h^2)$ error is approximately 0. Figure 1c shows a more exotic case, in which D is very large, D = 3.5 and α = 0. This case is strongly unstable to local modes and is not of primary interest in a global stability calculation. Figure 1c applies to the third unstable eigenmode. (Thus, there are two modes with more negative eigenvalues or larger growth rates). For the case of Fig. 1c, the best convergence is obtained for $p \approx 1$ which illustrates that the optimum value of p is case-dependent. It is important to note that in practical applications, the interesting range of D is rather narrow, say $|D| < 0.25$, and that in this range, the optimum p is almost constant ≈ 0.

The dependence of the error on p and on the system parameters can be seen by applying the error estimate (12) to the problem (13). This yields $\delta\lambda = \Lambda - \lambda = E / (-I)$, where

$$E = h^2 \left[\frac{1}{12} \int_{-1}^{1} (x^2 - \lambda)\, u''^2\, dx + \frac{1}{4} \left(p - \frac{1}{3}\right) (1 - D) \int_{-1}^{1} u'^2\, dx \right]$$

$$-I = \int_{-1}^{1} u'^2\, dx + \alpha\, u^2(-1) \qquad (14)$$

Equation (14) shows that in cases of practical interest, where $D < 1$, the approximate eigenvalue decreases (the discrete approximation becomes more unstable) when p decreases, and that the optimum p is less than 1/3. Note that for Eq. (13), the dominant contribution to E from the integration error comes from the $f''u'^2$ term rather than from the $2gu'^2$ term as in the introductory example. Since these two terms have the opposite sign, the optimal change of p away from the strict FEM value of 1/3 has the opposite sign for the two different problems.

Figure 2 shows the normalized error $c = -\delta\lambda/h^2$ obtained from numerical solution of (13) as points and the lines show the error estimate (14) using the numerically computed eigenfunctions. The good agreement confirms the correctness of (12). We see that c is a linear function of p and that its slope changes sign at D = 1, as predicted by (14). More importantly, for numerically small D, the best convergence is obtained for $p \approx 0$, which is consistent with the good performance of the hybrid finite elements (p = 0) in ideal MHD calculations.

4.1 Discussion

An example similar to Eq. (13) has been studied previously by Degtyarev and Medvedev [10]. These authors considered the method of adding a penalty function to the hybrid finite elements. It is clear from the error estimation formula (14) that the integration error may be seen as a penalty function $(p/4)\,(1-D)\int u'^2h^2\,dx$ added to the potential energy of the hybrid elements. Thus, an alternative point of view to the one presented here is that the tunable integration scheme gives a certain recipe for how to choose the penalty function. The simplicity of this recipe appears particularly useful in more complicated cases such as the resistive MHD system to be discussed in Sec. 5.

The curves for $D = \pm 0.1$ in Fig. 2 show that the hybrid finite elements (p = 0) give considerably better convergence than regular FEM (p = 1/3) for the ideal-MHD problem (13) when |D| is not too large. For MHD stability studies, convergence from the unstable side is usually preferable, at least for equilibria with a small number of resonant surfaces. This reduces the chances of not detecting weak instabilities, and sufficiently small upper bounds for the growthrates of numerically destabilized modes can easily be obtained by means of mesh accumulation around each resonant surface. On the other hand, in three-dimensional MHD stability calculations [11], the number of resonant surfaces can become very large and it is impractical to accumulate the mesh around each of them. For these cases, it is desirable to have a numerical algorithm that converges from the stable side. An advantage of our tunable

integration scheme is that it has enough flexibility to give either type of convergence simply by adjusting the integration parameter. We also note that in principle, application of the method to higher order elements is straightforward.

5. NUMERICAL EXAMPLE II - RESISTIVE MHD FORMULATION

For plasmas of finite electrical resistivity, the MHD system (13) is modified to read [12]

$$\gamma u'' = xj - Du/\gamma \quad , \tag{15a}$$

$$\gamma\psi = xu - \eta j \quad , \tag{15b}$$

$$0 = \psi'' + j \quad . \tag{15c}$$

Here, η denotes the resistivity, γ the growth rate, u the fluid velocity perpendicular to the equilibrium magnetic surfaces, ψ the magnetic flux perturbation, and j the perturbed electrical current. When $\eta = 0$ (15a-c) can be rewritten as (13) with $\lambda = -\gamma^2$, but whenever $\eta > 0$, it is necessary to introduce a dynamical variable ψ representing the magnetic field. We consider (15) on the interval [-1, 1] and choose $\eta = \eta_0 (1-x^2)^2$. (This makes the equation ideal at the end points and it suffices to specify boundary conditions for u.) The boundary conditions will be taken as $u'(-1) - \alpha u(-1) = 0$ and $u'(1) - \beta u(1) = 0$, and we will hold $\beta = -1$ fixed.

The resistive system (15) with $\eta > 0$ is non-selfadjoint. However, solution by the FEM is straightforward; u, ψ, and j are expanded as piecewise linear functions, and each of Eqs. (15a-c) is multiplied by an arbitrary piecewise linear weighting function. We shall refer to this as the standard solution. The integration will be carried out by the tunable scheme (3). As we will see, the tunable integration scheme works well for the standard method of solution.

However, as will also become apparent, there are alternative formulations for the problem (15) where the tunable integration method gives less satisfactory results. For instance, we have considered one modification of the system itself: in the term xj in (15a), j may be replaced by - ψ''. Although this does not change the equation in an analytical sense, it changes the discrete approximation. We indicate the form of the equation by a first index which is 1 for the form (15a) and 2 when j is replaced by - ψ''. Secondly, the FEM implementation is not unique: instead of piecewise linears, we can use Dirac delta functions on the grid points as weighting functions for Eq. (15b) so that this equation is solved by collocation. This modification will be indicated by a second index which is 1 for the piecewise linear weighting functions and 2 for the delta functions.

5.1 Ideal test cases

We first consider the ideal case $\eta = 0$ and take similar parameters as in Figs. 1a and 1b. The growthrate γ converges quadratically with h. The convergence parameter $c = \delta\gamma^2/h^2$ [analogous to that for Eq. (13)] is shown in Fig. 3 as a function of p for the four different discretizations. In Fig. 3a, $D = -0.1$, $\alpha = -0.13$, $\beta = -1$ with a converged $\gamma^2 \approx 2.404 \times 10^{-2}$, and in Fig. 3b, $D = 0.1$, $\alpha = 0.06$, and $\beta = -1$ with a converged $\gamma^2 \approx 1.119 \times 10^{-2}$.

Several features may be noted in Fig. 3. First, for the standard solution of the non-selfadjoint system (15), the dependence of c on p is *opposite* to the corresponding cases in Fig. 2, and the optimum p for both test cases is close to the 2/3. (More precisely $p_{opt} \approx 0.653$ in case (a) and $p_{opt} \approx 0.670$ in case (b).) For the standard solution, the hybrid elements perform poorly, and the rigorous FEM method should be modified in the opposite sense by increasing p towards finite differences. [For an inhomogeneous equation, p = 1 does not necessarily lead to the finite difference formula, even on an equidistant grid, as is evident for Eq. (13). However, for Eq. (15), p = 1 does give the same result as finite differences. Note also that for p = 1, the four different solution methods for (15) are identical so that $c_{11}(1) = c_{12}(1) = c_{21}(1) = c_{22}(1)$.]

Second, the results of the standard solution are changed in almost an identical way when either the xj term in (15a) is replaced by $-x\psi''$ or Eq. (15b) is solved by collocation. With either modification, the slope dc/dp is about the half of that for the standard solution, and optimum convergence is obtained for $p \approx 1/3$.

Third, with both modifications included, the convergence curves are almost independent of p, as seen from the curves for $c_{22}(p)$. This is as expected, since (with the exception of the numerically small D term) all integrations needed for the discretization are now exact by either the trapezoidal or midpoint rules. Figure 3 shows that the solution method (2,2) generally behaves rather poorly and that the p required to make $c_{22} = 0$ is numerically large and even has opposite signs for the two test cases. The fact that the most important integrations are exact means that the solution cannot be improved by the tunable integration. Stated differently, the tunable integration scheme is useful only when the integrations are not exact !

The differences shown in Fig. 3 between the four treatments of Eq. (15) have also been borne out by an error analysis based on a symmetric quadratic form constructed from Eq. (15). This will be discussed in a future publication.

5.2 Resistive test cases

The purpose of the non-selfadjoint formulation (15), where the magnetic field appears as a variable, is of course to compute resistive, rather than ideal, modes. For the discussion of the numerical test cases, we quote some analytical results [12] for (15), valid in the limit of small resistivity. For sufficiently small values of |D|, so called tearing modes are unstable if and only if $\Delta' = (\psi'_+ - \psi'_-) / \psi(0)$ is positive. (ψ'_+ and ψ'_- are the derivatives of ψ evaluated just outside a resistive layer of width $\propto \eta^{2/5}$.) These global modes are slowed down, but not completely stabilized, by a negative D, and are sped up by a positive D. The required magnitude of D to affect the growthrate significantly is $(\eta^{1/3}\Delta')^{6/5}$. When $0 < D < 1/4$, there

are infinite sequences of unstable local modes, called resistive interchanges, and the most unstable of these may be connected to a global mode.

Figure 4 shows $c(p) \equiv [\gamma(h) - \gamma(0)]/h^2$ for two test cases that are ideally stable but resistively unstable. The example shown in Fig. 4a has $D = 0.1$, $\eta = 2 \times 10^{-3}$, $\alpha = 0.6$ and $\beta = -1$. The unstable mode is a mixture of tearing and resistive interchange with a converged growthrate of $\gamma \approx 3.326 \times 10^{-2}$. As shown by Fig. 4, it is only the standard method of solution (1,1) that gives $c(p) = 0$ for p between 0 and 1. (Outside this interval, some of the integration weights become negative, which appears undesirable.) For the standard solution, $c(p) = 0$ is obtained for $p \approx 0.669$, which is remarkably close to the 2/3 of the introductory example.

The case shown in Fig. 4b has $D = -0.1$, $\eta = 2 \times 10^{-3}$, $\alpha = 0.2$ and $\beta = -1$. Here, the external driving is stronger than in 4a (α is smaller), but the growth is weaker because of the stabilizing influence of favorable curvature, $D < 0$. The converged growthrate is $\gamma \approx 1.160 \times 10^{-2}$. Also in this case, only the standard solution achieves $c(p) = 0$ for p between 0 and 1. The optimum p is about 0.75. For this example, convergence in some cases is more difficult than is apparent from Fig. 4b. Specifically, for the smallest value of p used in the study (=0.02), the methods where (15b) is projected on tent functions give convergence curves γ vs h^2 that are far from an asymptotic straight line even with 100 grid points.

5.3 Discussion

From the convergence rates shown in Figs. 3 and 4, we conclude that the best convergence for the resistive system (15) is obtained by the standard method of solution and the tunable integration scheme with p close to 2/3. This is similar to the result for the simple introductory example $u'' + \lambda u = 0$. Furthermore, in both these cases, the numerical approximation of the eigenvalue (in the first case λ , in the second case $-\gamma^2$) is larger the smaller p is. Stated differently, the eigenvalues of the 'stiffness matrix' increase, or the numerical approximation becomes more stable (in the physics sense) with decreasing p. It

appears plausible that the reason for this similarity is that the second order differentiation that is central in defining the potential energy of the system, is carried out in the same manner in the two cases [compare Eq. (1), $u'' + \lambda u = 0$, with Eq. (15c), $\psi'' + j = 0$].

However, it should be noted that for the ideal problem in the non-selfadjoint formulation, we found two alternative discretizations for which the optimum p is close to 1/3. Finally, for the selfadjoint formulation (13) of the ideal problem, the optimum p is close to 0. Thus, *the optimum value of* p *is strongly dependent on the form of the equation.* The hybrid elements [6] with $p = 0$ are evidently very well tailored to the selfadjoint ideal formulation (13), but do not perform well on the u-ψ representation of the resistive MHD system (15). Conversely, the finite difference-like scheme $p = 1$ is reasonably accurate on the resistive formulation (15) but performs poorly on the ideal system (13). In both cases, the strict finite element method is intermediate.

6. CONCLUSION

We have shown that the convergence rate for the finite element method can be improved by using a modified integration scheme with a tunable parameter p. The tunable integration scheme is simple to implement and can be applied to a wide class of problems.

In the present paper, the method has been tested on three different eigenvalue problems solved by piecewise linear elements. In each case, it has been possible to find values of p that clearly improve the convergence over the strict FEM and nearly eliminate the $O(h^2)$ error of the eigenvalue. The two numerical examples we have discussed in Eqs. (13) and (15) contain free parameters, and the precise rate of convergence depends on the values of the parameters. However, for each of the two problems, the range of practical interest for these parameters is limited, and *throughout this range, the optimum* p *is almost constant.* (In the case of Eq. (15) this holds only for the standard solution.) Thus, at least for certain systems of equations and suitable finite element representations, the integration parameter can be fixed, and need not be

adjusted for every case. We emphasize that *the optimum* p *is different for different types of equation.* This is clearly shown by our two numerical examples in Secs. 4 and 5, where $p_{opt} \approx 0$ for the ideal equation (13) while $p_{opt} \approx 2/3$ for the resistive system (15).

We find the results obtained with the tunable integration method encouraging. A main advantage of the method is that it gives an external knob that can be used to modify the convergence properties according to what is most practical for a given application. The ideas presented here grew out of discussions concerning the convergence properties of two recently developed MHD stability codes, the three-dimensional ideal code TERPSICHORE [11] and the two-dimensional resistive code MARS [13] and attempts to control these convergence properties. The method has been incorporated into the two codes and the results will be reported elsewhere.

REFERENCES

[1] G. Strang and G.J. Fix, *An analysis of the finite element method* (Prentice-Hall, Englewood Cliffs, N.J., 1973)

[2] T.J.R. Hughes, *The finite element method* (Prentice-Hall, Englewood Cliffs, N.J., 1987)

[3] K. Appert, D. Berger, R. Gruber, F. Troyon and J. Rappaz, Z. Ang. Math. Phys. **25** (1974) 229.

[4] X. Llobet, K. Appert, A. Bondeson and J. Vaclavik, Comput. Phys. Comm. **59** (1990) 199.

[5] R.D. Richtmeyer and K.W. Morton, *Difference methods for initial value problems*, 2nd ed (Interscience, New York, 1967).

[6] R. Gruber, F. Troyon, D. Berger et al, Comput. Phys. Comm. **21** (1981) 323.

[7] W.A. Newcomb, Ann. Phys. **10** (1960) 232.

[8] B.R. Suydam, in *Proceedings of Second International Conference on the Peaceful Uses of Atomic Energy*, Geneva (United Nations, Geneva, 1958), p.157.

[9] C. Mercier, Nucl. Fusion **1** (1960) 47.

[10] L.M. Degtyarev and S. Yu. Medvedev, Comput. Phys. Comm. **43** (1986) 29.

[11] W.A. Cooper, G.Y. Fu, R. Gruber, S. Merazzi, U. Schwenn and D. Anderson, in *Theory of Fusion Plasmas*, Proc. Workshop Varenna 1990 (Editrice Compositori, Bologna, to be published 1991).

[12] B. Coppi, J.M. Greene, and J.L. Johnson, Nucl. Fusion **6** (1966) 101.

[13] A. Bondeson, G. Vlad and H. Lütjens, in *Controlled Fusion and Plasma Physics*, Proc. 17th European Conf., Amsterdam 1990 (European Phys. Soc., Geneva, 1990), Part II, p. 906.

FIGURE CAPTIONS

FIGURE 1 Numerical eigenvalue Λ vs. square of the cell size h for the ideal-MHD system (13). In (a) D = - 0.1 and α = - 0.13, and in (b) D = 0.1 and α = 0.06. (c) refers to the third most unstable mode for D = 3.5 and α = 0 . The curves are labeled by the values of the integration parameter p.

FIGURE 2 Normalized error in the eigenvalue $c = -(\Lambda(h) - \lambda_{exact})/h^2$ as functions of the integration parameter p for the three cases shown in Figs. 1a-c. Also shown is the case D = 1 and α = 0, for which the error is independent of p, cf Eq. (14). The discrete points show results from numerical convergence tests and the lines represent the error estimate (14) with the numerically computed eigenfunctions.

FIGURE 3 Normalized error in the growthrate $c = (\gamma^2(h) - \gamma^2_{exact})/h^2$ as functions of the integration parameter p for ideal MHD instabilities computed from the non-selfadjoint formulation (15). In (a) D = - 0.1, α = - 0.13 and β = - 1 and in (b) D = 0.1, α = 0.06 and β = - 1. The curves are labeled according to the different solution methods described in Sec. 5.

FIGURE 4 Normalized error in the growthrate $c = (\gamma(h) - \gamma_{exact})/h^2$ as functions of the integration parameter p for resistive MHD instabilities of (15). In (a) $\eta_0 = 2 \times 10^{-3}$, D = 0.1, α = 0.6 and β = -1 and in (b) $\eta_0 = 2 \times 10^{-3}$, D = - 0.1, α = 0.2 and β = -1.

Figure 1a

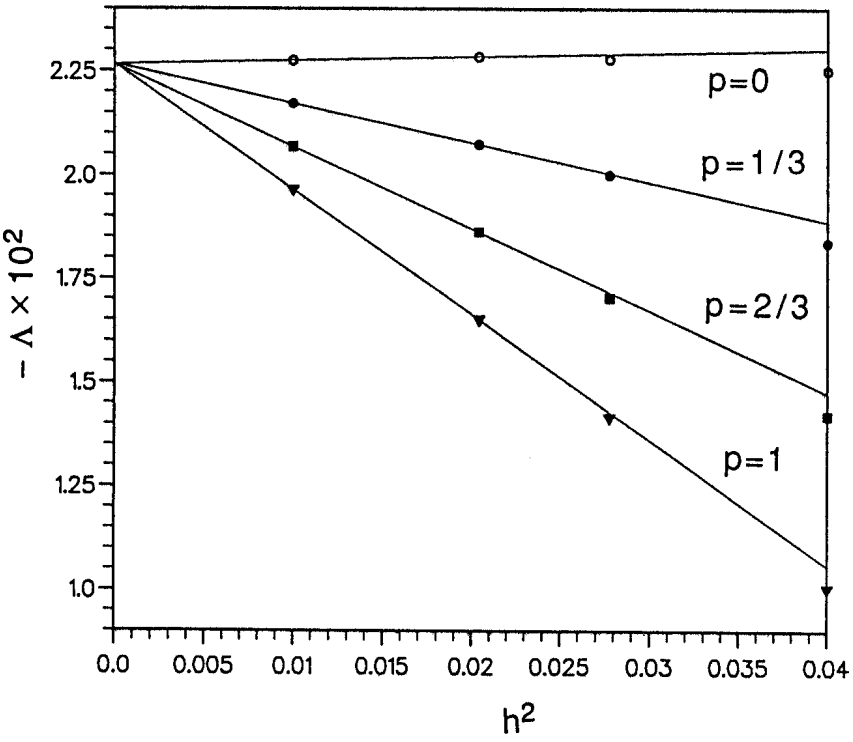

Figure 1b

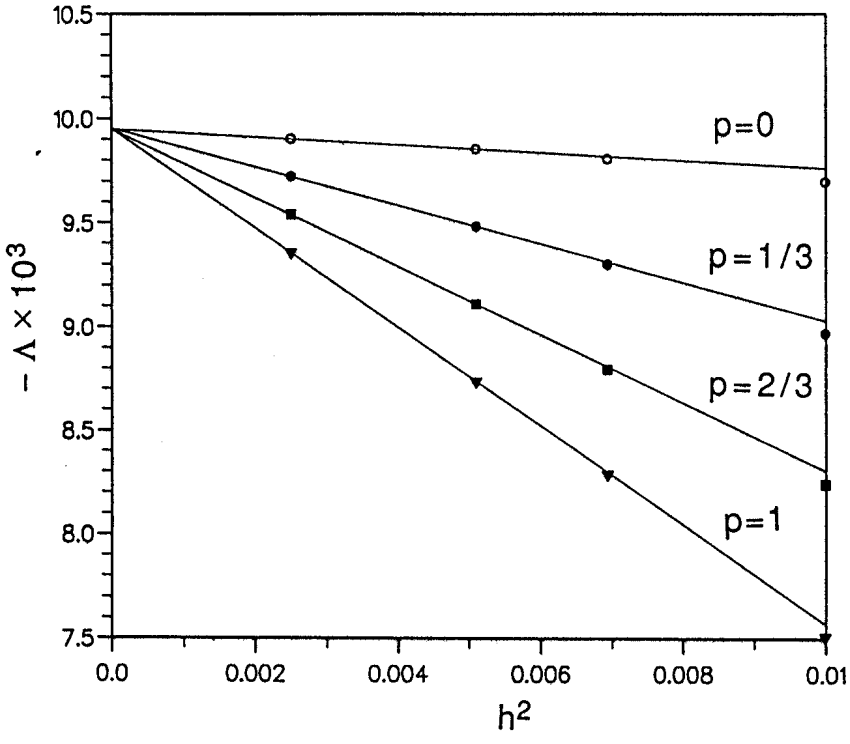

Figure 1c

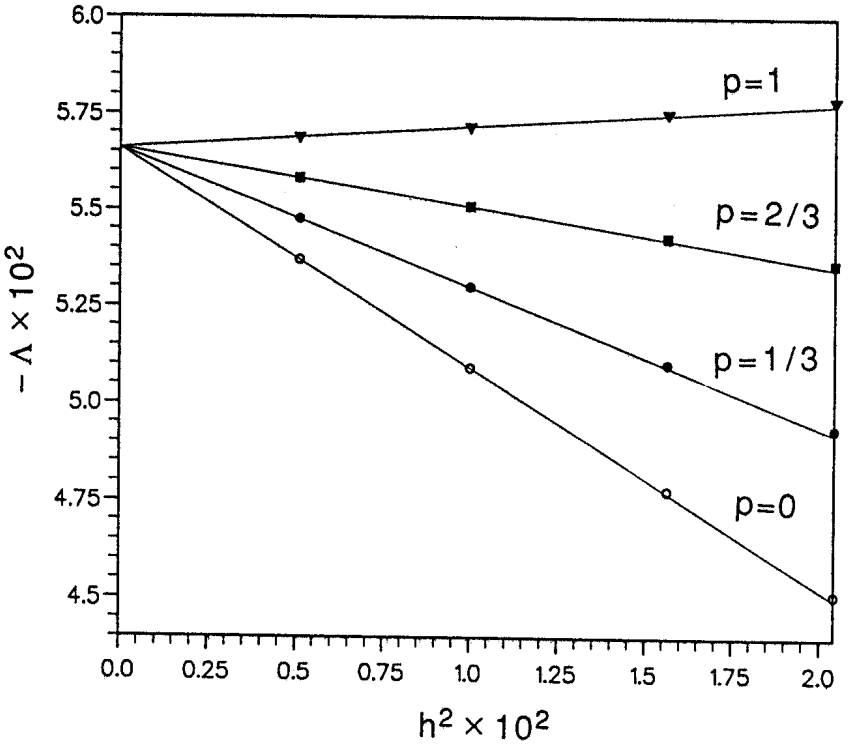

Figure 2

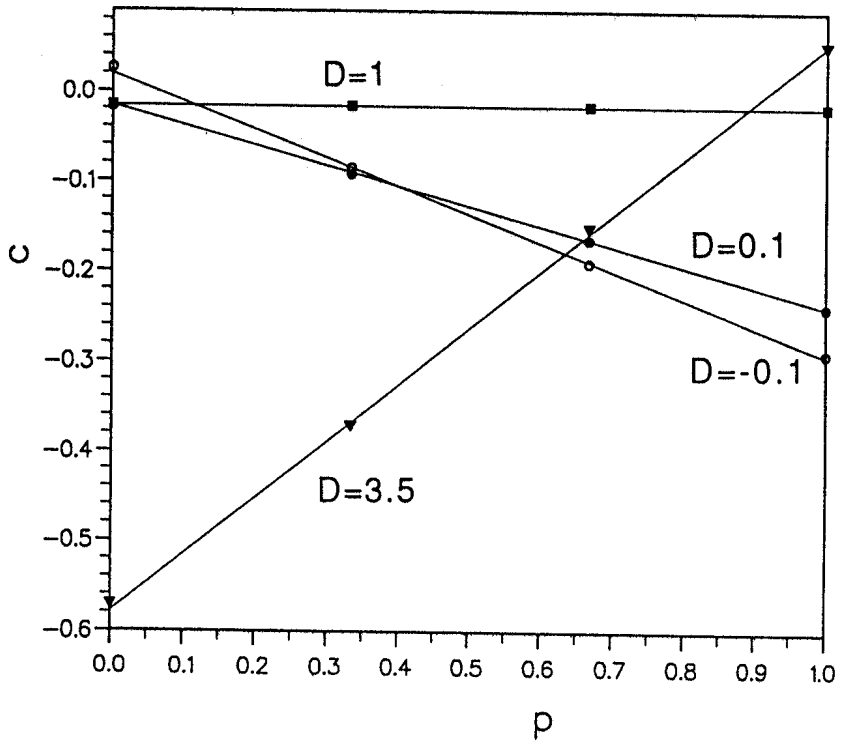

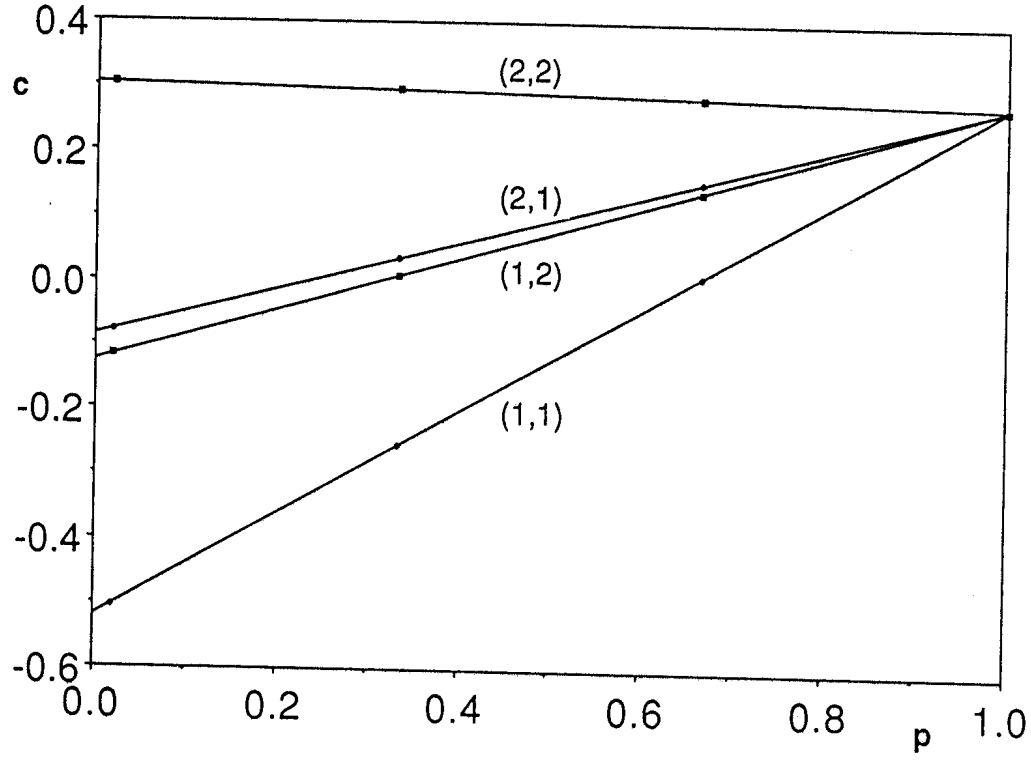

Figure 3a

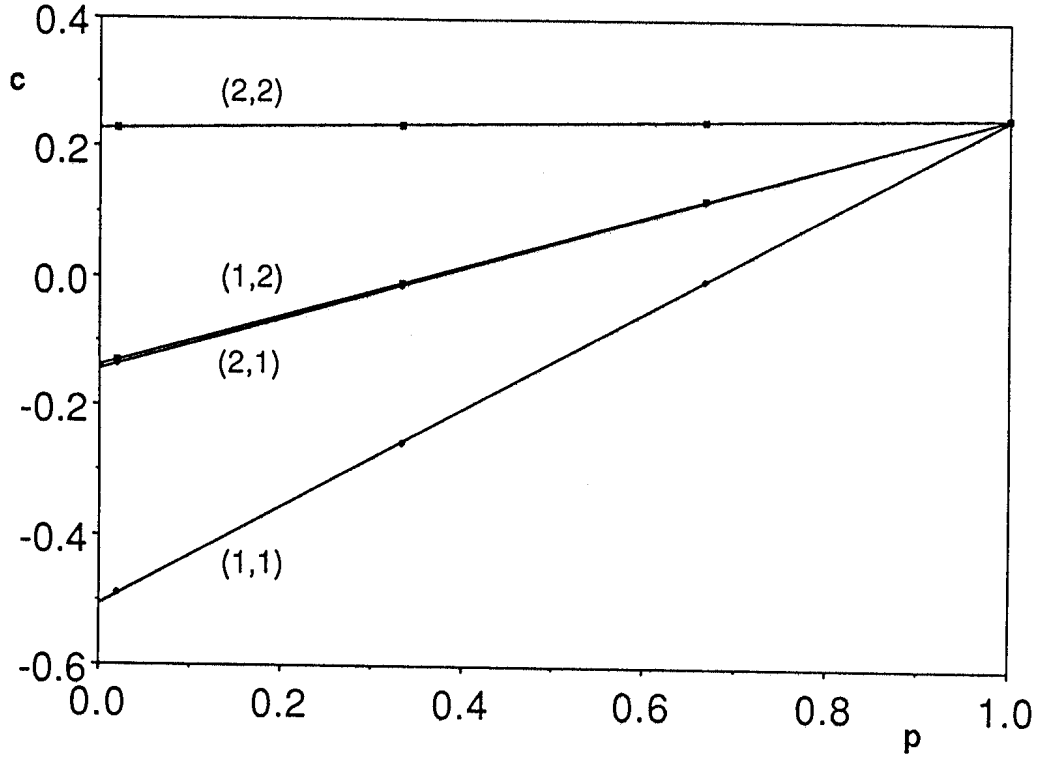

Figure 3b

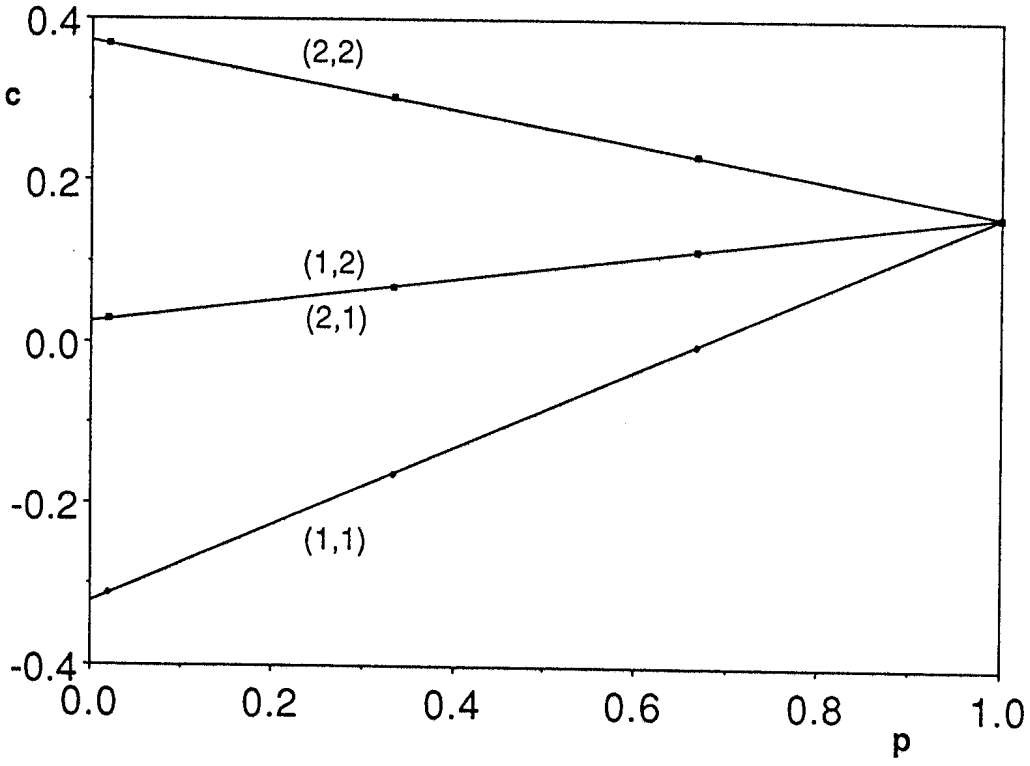

Figure 4a

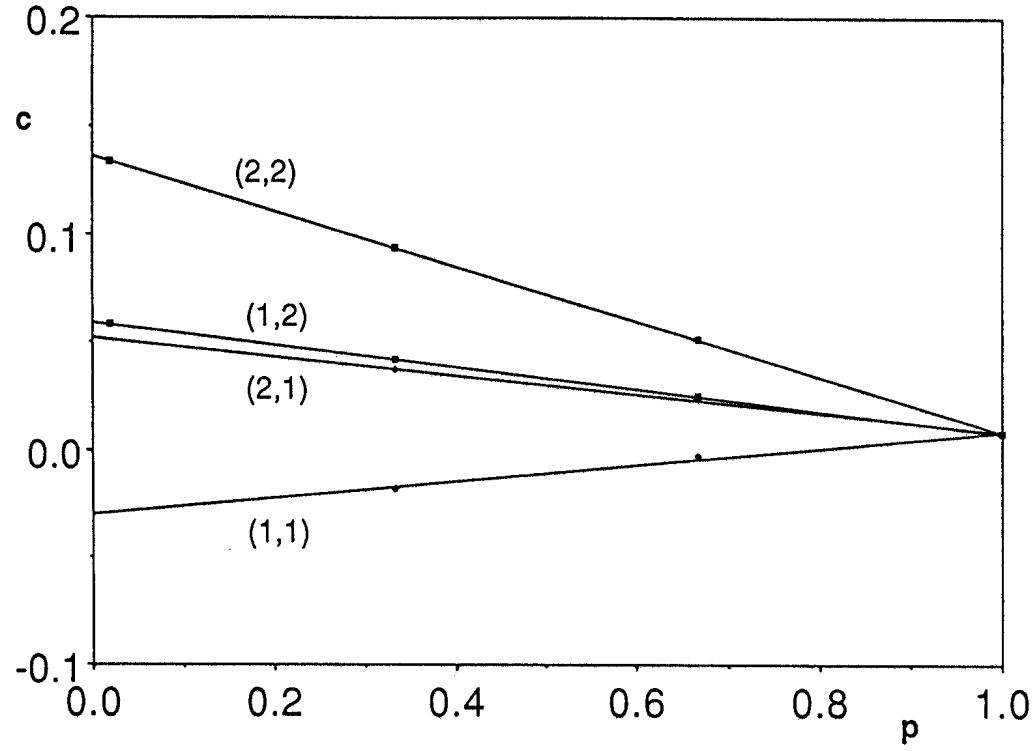

Figure 4b